LETTERS

2,000-year-long temperature and hydrology reconstructions from the Indo-Pacific warm pool

Delia W. Oppo[1], Yair Rosenthal[2] & Braddock K. Linsley[3]

Northern Hemisphere surface temperature reconstructions suggest that the late twentieth century was warmer than any other time during the past 500 years and possibly any time during the past 1,300 years (refs 1, 2). These temperature reconstructions are based largely on terrestrial records from extra-tropical or high-elevation sites; however, global average surface temperature changes closely follow those of the global tropics[3], which are 75% ocean. In particular, the tropical Indo-Pacific warm pool (IPWP) represents a major heat reservoir that both influences global atmospheric circulation[4] and responds to remote northern high-latitude forcings[5,6]. Here we present a decadally resolved continuous sea surface temperature (SST) reconstruction from the IPWP that spans the past two millennia and overlaps the instrumental record, enabling both a direct comparison of proxy data to the instrumental record and an evaluation of past changes in the context of twentieth century trends. Our record from the Makassar Strait, Indonesia, exhibits trends that are similar to a recent Northern Hemisphere temperature reconstruction[2]. Reconstructed SST was, however, within error of modern values from about AD 1000 to AD 1250, towards the end of the Medieval Warm Period. SSTs during the Little Ice Age (approximately AD 1550–1850) were variable, and ~0.5 to 1 °C colder than modern values during the coldest intervals. A companion reconstruction of $\delta^{18}O$ of sea water—a sea surface salinity and hydrology indicator—indicates a tight coupling with the East Asian monsoon system and remote control of IPWP hydrology on centennial–millennial timescales, rather than a dominant influence from local SST variation.

The IPWP is the largest reservoir of warm surface water on the Earth and the main source of heat for the global atmosphere. Small variations in SST of the IPWP influence the location and strength of convection in the rising limb of the Hadley and Walker circulations, and can thus perturb planetary-scale atmospheric circulation and influence tropical hydrology[4]. However, tropical hydrology is also responsive to high-latitude temperature change[5,6]. Recent work suggests that SST of the IPWP has varied during the past millennium, with colder SSTs during the peak of the Little Ice Age (LIA) than during the preceding centuries[7]. However, no millennial-length SST reconstructions from the IPWP capture the complete warming out of the LIA or extend into the instrumental era to allow a direct comparison with instrumental data. Therefore, the amplitude of reconstructed SST variations in the context of modern SSTs is still uncertain. Whereas conventional sediment corers—gravity and piston corers—often disturb surface and latest Holocene sediments, multi-corers are lowered gently into ocean sediment and recover the sediment–water interface undisturbed, together with about a half-metre of underlying sediment. Combining records from multi-cores and gravity or piston cores enables the reconstruction of long records that overlap the instrumental record.

We worked on multi-core BJ8-03-31MCA ('31MC') and gravity cores BJ8-03-32GGC ('32GGC') and BJ8-03-34GGC ('34GGC'), recovered from the Makassar Strait, on the Sulawesi margin (Fig. 1). We also use published data from nearby piston core MD98-2160[7] ('MD60'). Mean annual SSTs in our study area averaged ~29.3 °C from 1997 to 2007 (ref. 8) with coldest SSTs (averaging ~28.5 °C) from July through to the end of September (JAS), the upwelling season. SSTs decrease during El Niño events[4,8]. Seasonally, surface waters are freshest in boreal winter, when SST is warmest, owing to the combined influence of the northwest monsoon/intertropical convergence zone rainfall[9,10] and advection of low salinity waters to the site by surface currents (Supplementary Discussion). Boreal summer precipitation is reduced during El Niño events, but rainy season precipitation is unaffected[10]. The mean annual weighted $\delta^{18}O$ value of precipitation ($\delta^{18}O_{ppt}$) is close to the boreal winter value (about −7‰ versus approximately −4‰ in boreal summer[11]), reflecting intense vertical convection and heavy rainfall[12]. Sediment core chronologies

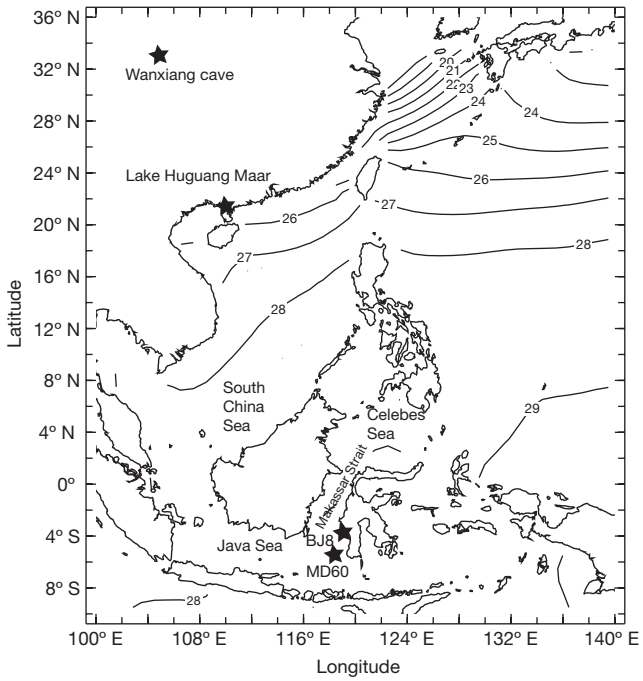

Figure 1 | Mean annual SST of the IPWP. Shown (stars) are locations of sediment cores as follows: multi-core BJ8-03-31MCA (459 m), and gravity cores BJ8-03-34GGC (503 m) and BJ8-03-32GGC (454 m), all at 3° 53′ S, 119° 27′ E ('BJ8'), and piston core MD98-2160 (5° 12′ S, 117° 29′ E, 1,185 m, 'MD60'). Locations of Lake Huguang Maar and Wanxiang cave are also shown (stars). Temperature data from ref. 29.

[1]Department of Geology and Geophysics, Woods Hole Oceanographic Institution, Woods Hole, Massachusetts 02543, USA. [2]Institute of Marine and Coastal Sciences, and Department of Earth and Planetary Sciences, Rutgers, The State University, New Brunswick, New Jersey 08901, USA. [3]Department of Atmospheric and Environmental Sciences, University at Albany–State University of New York, Albany, New York 12222, USA.

are based on ^{210}Pb (31MC), radiocarbon dating, and a correlation to the AD 1815 Mount Tambora ash tentatively identified in MD60[7] (Supplementary Methods). High sediment accumulation rates (~100–200 cm kyr^{-1}) enable decadal-scale resolution. To reconstruct $\delta^{18}O$ of sea water (SST and $\delta^{18}O_{sw}$), we generated Mg/Ca and $\delta^{18}O$ data on the planktonic foraminifera, *Globigerinoides ruber* (sensu stricto morphotype), which inhabits the surface mixed layer (Methods). Sediment trap data indicate that in the tropics, the seasonal preference of *G. ruber* varies among locations, ranging from a cold season (upwelling) preference to a warm season preference[13–15] (Supplementary Discussion).

We converted Mg/Ca to SST using a calibration, Mg/Ca = 0.38exp(0.09SST), based on seasonal Mg/Ca variations in multiple species of planktonic foraminifera from Sargasso Sea sediment trap samples[16] (Fig. 2a). Our reconstructed SSTs generally fall between historical mean annual and JAS SSTs (the National Oceanic and Atmospheric Administration extended SST reconstruction[8], ERSSTv3; Fig. 2), suggesting that the seasonal flux of *G. ruber* to the sediment (*G. ruber* seasonality) in our study area varied through time, with a greater flux to the sediment in JAS during cooler periods (for example, around AD 1900–50) relative to warm periods, when reconstructed SSTs approach the annual mean.

We applied the Mg/Ca–SST calibration[16] to data from all four cores (Fig. 2b). Following previous studies[7,17–19], we also reconstructed

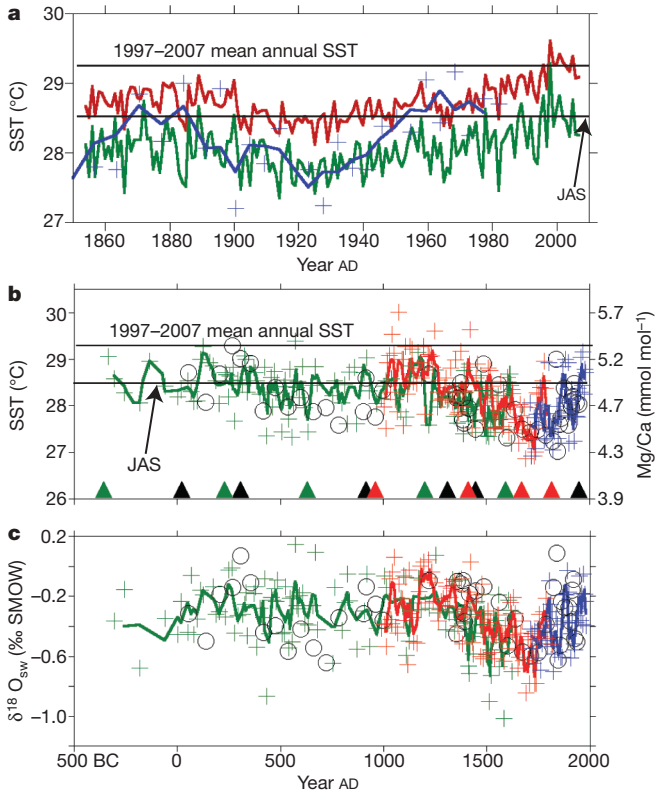

Figure 2 | Sea surface temperature and $\delta^{18}O_{sw}$ reconstructions. **a**, ERSSTv3[8] mean annual (red line) and JAS (green line) SST reconstructions based on the instrumental record for the grid box containing the BJ8 core sites. Blue line, Mg/Ca-based SST estimates using a published calibration[16]. Crosses, Mg/Ca-based SST estimates. Lines are three-point running means. **b**, Downcore SST, and **c**, $\delta^{18}O_{sw}$ reconstructions (31MC, blue crosses; MD60, red crosses; 34GGC, green crosses; 32GGC black circles). Colour-coded lines are three-point running means. Upper and lower horizontal lines in **a** and **b** are modern (1997–2007) mean annual and JAS SST[8] at the BJ8 core sites, respectively. Colour-coded triangles in **b** denote radiocarbon age control, except for the most recent red triangle, which denotes the Mt Tambora ash, tentatively identified in MD60 (Supplementary Notes). $\delta^{18}O_{sw}$ values are relative to Vienna Standard Mean Ocean Water (VSMOW).

$\delta^{18}O_{sw}$ from the $\delta^{18}O$ of *G. ruber* (Supplementary Data) and our SST estimates (Fig. 2c). The SST reconstruction shows cooler temperatures between about AD 400 and AD 950 than during much of the so-called Medieval Warm Period (about AD 900–1300), a warm period found in many northern high-latitude records but whose global significance is uncertain[1]. A gradual SST decrease began at about AD 1300, and culminated at about AD 1700, within the peak of the LIA. Subsequent warming was interrupted by two multi-decadal cold periods, one towards the end of the LIA and one during the early twentieth century. Each was nearly as cold as the coldest LIA peak.

At face value, our reconstruction suggests that peak LIA SSTs were ~1 °C and 1.5 °C colder than late twentieth century JAS and mean annual SST, respectively. Given the possibility raised by our comparison of reconstructed SST to the instrumental record (Fig. 2a) that the flux of *G. ruber* to the sediment was higher in JAS during the LIA than at present, we favour a conservative interpretation that JAS surface waters were ~1 °C colder than late twentieth century JAS SSTs. Considering that from 1856 to 2007[8], the amplitude of mean annual SST variability averaged ~70% of the amplitude of JAS SSTs variability (Supplementary Discussion), we infer that mean annual SSTs were ~0.5 to 1 °C colder than the late twentieth century.

Reconstructed SSTs were warmest from AD 1000 to AD 1250 and during short periods of first millennium (Fig. 2b). Given the evidence that *G. ruber* tends to record near mean annual SSTs during warm intervals of the last 150 years (Fig. 2a), reconstructed SSTs during these warm periods probably reflect mean annual SSTs. If this is the case, as we suspect, then SSTs within error of modern SSTs occurred in the IPWP during the Medieval Warm Period and during brief periods of the first millennium AD. If, on the other hand, *G. ruber* calcified preferentially during the JAS upwelling season throughout the study interval, then JAS SSTs as warm as modern also characterized the previous millennium. Regardless of *G. ruber* seasonality in this region, the reconstruction suggests that at least during the Medieval Warm Period, and possibly the preceding 1,000 years, Indonesian SSTs were similar to modern SSTs.

To estimate errors and facilitate comparison to other records, we developed composite records (Fig. 3; Methods Summary). Our averaging scheme reduces the amplitude of the records, but preserves only the most robust features. Considering the age uncertainties in our reconstruction, long-term SST trends are similar to those in Northern Hemisphere temperature reconstructions, especially the 'NH land error-in-variables (EIV) composite'[2] ($r^2 = 0.5$, $P \ll 0.00001$; Fig. 3a), consistent with the instrumental record, which suggests that Indonesian SST is correlated to global SST and air temperature on multi-decadal and longer timescales (Supplementary Notes). (Here NH indicates Northern Hemisphere.) Contrary to the Indonesia SST reconstruction, however, the Northern Hemisphere temperature reconstruction does not estimate temperatures as warm as modern at any time during the past two millennia. The hemispheric and global temperature difference between the early AD 1900s and the modern era is similar to the difference in mean annual SST at our core site (Supplementary Notes), so the greater amplitude of Makassar Strait SST than Northern Hemisphere temperature variability (note different axis scaling in Fig. 3a) may be related to the hypothesized changes in *G. ruber* seasonality. We note that the high-amplitude variations resulting from these hypothesized changes in *G. ruber* seasonality also preclude accurate estimates of the rates of SST change in the past and a meaningful comparison to the rate of SST increase during the past decade.

Long-term $\delta^{18}O_{sw}$ trends are also similar to Northern Hemisphere temperature trends ($r^2 = 0.3$, $P \ll 0.0001$) with the lowest values during the coldest peak of the LIA (Fig. 3b). The $\delta^{18}O_{sw}$ decrease that began at about AD 1300 was linked to gradual Northern Hemisphere and IPWP cooling, and the subsequent increase in $\delta^{18}O_{sw}$ values associated with nineteenth- and twentieth-century warming. This general trend of increasing $\delta^{18}O_{sw}$ was punctuated by two multi-decadal $\delta^{18}O_{sw}$ minima, each with slightly higher $\delta^{18}O_{sw}$ values. By

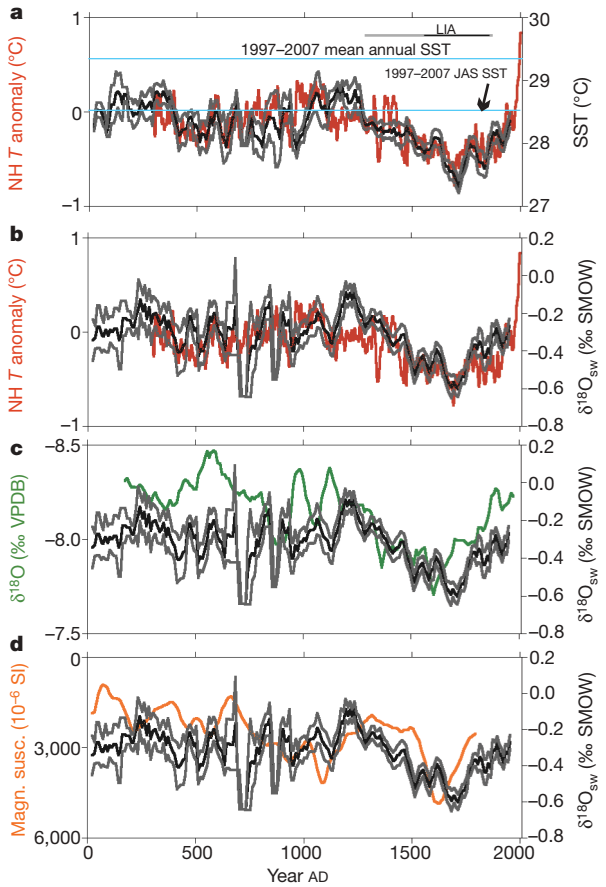

Figure 3 | Comparison of composite Indonesia records to hemispheric and regional records. **a**, Composite SST and **b**, $\delta^{18}O_{sw}$ records (black) versus Northern Hemisphere land EIV composite temperature (T) anomaly[2] (red). **c**, Composite $\delta^{18}O_{sw}$ record (black) versus $\delta^{18}O$ of Wanxiang cave, a summer monsoon record[23] (green) and **d**, Lake Huguang Maar magnetic susceptibility, a winter monsoon record[24] (orange). Upper and lower horizontal lines in **a** are modern (1997–2007) mean annual and JAS SST[8] at the BJ8 core sites, respectively. Composite records were developed by averaging data in 10-year overlapping, 50-year-long bins. Error bars (grey), ±1 standard error of data in each bin. Wanxiang cave and Lake Huguang Maar data were also averaged in 10-year overlapping 50-year bins for clarity. The approximate time interval of the Little Ice Age (LIA) is denoted by the horizontal bar in **a**.

analogy with the seasonality of modern precipitation[9,10], of $\delta^{18}O_{ppt}$ values[11,12], and of surface currents (Supplementary Discussion), the low $\delta^{18}O_{sw}$ values indicate that the Indonesian rainfall regime from about AD 1500 to AD 1900 was more boreal winter-like (stronger boreal winter, weaker boreal summer monsoon) than the preceding centuries.

Additional proxy evidence, discussed below, that the boreal summer monsoon was weaker during the LIA than during the Medieval Warm Period suggests that the colder surface waters implied by our record were not caused by greater monsoon-driven upwelling. El Niño events, as recorded in lake sediments from high-altitude Ecuador[20] and Galapagos[21], may have been subdued during the LIA, suggesting that neither a higher frequency/greater intensity of El Niño events nor a more El Niño-like mean Pacific state caused cold LIA SSTs. Rather, cooling of North Pacific surface water, which enters the southern Makassar Strait in boreal winter via the South China Sea/ Java Sea pathway to the west[4,22], is the likely proximal cause of LIA cooling.

Our interpretation of a more winter-like rainfall regime during the LIA is substantiated by records from Wanxiang cave, subtropical China[23] ($r^2 = 0.2$, $P \ll 0.0001$) and Lake Huguang Maar, coastal southeast China[24] ($r^2 = 0.1$, $P \ll 0.0001$) (Fig. 3c and d), which indicate weaker summer and stronger winter Asian monsoons, respectively, during the LIA. Low Indian summer monsoon rainfall[25] also corresponds to low $\delta^{18}O_{sw}$ (greater Indonesian rainfall) on

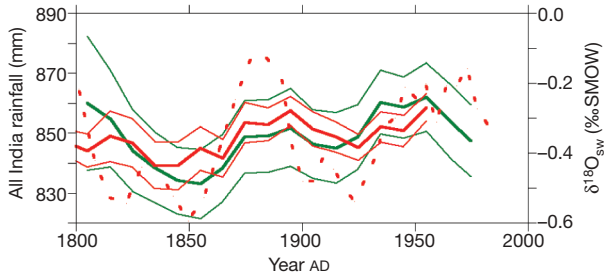

Figure 4 | Comparison of Indonesian $\delta^{18}O_{sw}$ and Indian rainfall. Red dashed line, 31MC $\delta^{18}O_{sw}$ three-point running mean; red solid lines, composite $\delta^{18}O_{sw}$ record (thick line) with ±1 standard error (thin lines); green, All India Rainfall index[25], 10-year overlapping, 50-year long bins (thick line), with ±1 standard error (thin lines).

multi-decadal timescales (Fig. 4) ($r^2 = 0.6$, $P < 0.0005$). These results, suggesting alternating precipitation maxima in the Northern Hemisphere Asian monsoon regions and over Indonesia, add to a growing body of evidence that monsoon/intertropical convergence zone variations profoundly influenced the tropical hydrology of the past two millennia[7,23,24,26,27].

Modern observations and modelling studies indicate that small changes in IPWP SSTs strongly influence the global hydrologic cycle[4]. For example, cooler SSTs in some areas of the IPWP might dampen intense deep atmospheric convection, reducing global precipitation[28]. However, our finding that $\delta^{18}O_{sw}$ was lowest (and by inference, net regional precipitation greatest) when SSTs were cold—during the LIA (Fig. 3) and the early AD 1900s (Fig. 4)—suggests that on multi-decadal through to millennial timescales, IPWP precipitation anomalies are not driven by local SST anomalies, but are remotely forced by the Asian monsoon/intertropical convergence zone.

METHODS SUMMARY

$\delta^{18}O$ and Mg/Ca were collected on *G. ruber* in the 212–250 μm and 250–300 μm size-fraction, respectively. $\delta^{18}O$ was measured at WHOI on a Finnigan MAT253 stable isotope mass spectrometer with the Kiel III Carbonate Device. Long-term precision of $\delta^{18}O$ measurements of standards is 0.07‰. Mg/Ca measurements were made at Rutgers Inorganic Analytical Laboratory using a sector field inductively coupled plasma mass spectrometer (Thermo Element XR). Additional details, including interlaboratory offsets and corrections, are discussed in Methods.

To construct composite records, we binned data from all four cores in 10-year-overlapping 50-year-long bins. We estimated errors in two ways. First, we took the standard error of the SST or $\delta^{18}O_{sw}$ in each 50-year bin (grey lines in Fig. 3). Second, we estimated errors by dividing the standard error in the SST and $\delta^{18}O_{sw}$ estimate by the square root of the number of data points in each bin. The standard error in the SST calibration is 0.16 °C. The standard error of the $\delta^{18}O_{sw}$ is a function of the error in both $\delta^{18}O$ of calcite and the error in SST. Assuming greater variance for geological samples than standards, we use a 0.2‰ standard deviation for the $\delta^{18}O$ of calcite, and knowing the standard error in the SST calibration, a standard error of 0.24‰ is estimated for $\delta^{18}O_{sw}$. The two methods gave similar error estimates for SST, but the second method (data not shown; http://www.ncdc.noaa.gov/paleo/) often suggests larger errors for $\delta^{18}O_{sw}$.

To estimate correlation coefficients and P values for the records shown on Figs 3 and 4, we linearly regressed data from each of the two records, already averaged within 10-year-overlapping 50-year-long bins.

Received 6 December 2008; accepted 15 June 2009.

1. Jansen, E. *et al.* in *Climate Change 2007: The Physical Science Basis* (eds Solomon, S. *et al.*) 466–482 (Cambridge Univ. Press, 2007).
2. Mann, M. E. *et al.* Proxy-based reconstructions of hemispheric and global surface temperature variations over the past two millennia. *Proc. Natl Acad. Sci. USA* **105**, 13252–13257 (2008).
3. National Research Council. *Surface Temperature Reconstructions for the Last 2,000 Years* (National Academy Press, 2006); available at ⟨http://www.nap.edu/catalog.php?record_id=11676⟩.
4. Qu, T., Du, Y., Strachan, J., Meyers, G. & Slingo, J. Sea surface temperature and its variability in the Indonesian region. *Oceanography* **18**, 50–61 (2005).
5. Broccoli, A. J., Dahl, K. A. & Stouffer, R. J. Response of the ITCZ to northern hemisphere cooling. *Geophys. Res. Lett.* **33**, doi:10.1029/2005GL024546 (2006).

6. Chiang, J. C. H. & Bitz, C. M. Influence of high latitude ice cover on the marine Intertropical Convergence Zone. *Clim. Dyn.* **25,** 477–496 (2005).
7. Newton, A., Thunell, R. & Stott, L. Climate and hydrologic variability in the Indo-Pacific Warm Pool during the last Millennium. *Geophys. Res. Lett.* **33,** L19710, doi:10.1029/2006GL0273234 (2006).
8. Smith, T. M., Reynolds, R. W., Peterson, T. C. & Lawrimore, J. Improvements to NOAA's historical merged land-ocean surface temperature analysis (1880–2006). *J. Clim.* **21,** 2283–2296 (2008).
9. Xie, P. & Arkin, P. A. Analyses of global monthly precipitation using gauge observations, satellite estimates, and numerical model predictions. *J. Clim.* **9,** 840–858 (1996).
10. Aldrian, E. & Susanto, R. D. Identification of three dominant rainfall regions within Indonesia and their relationship to sea surface temperature. *Int. J. Clim.* **23,** 1435–1452 (2003).
11. International Atomic Energy Agency/World Meteorological Organization. GNIP programme: resources. ⟨http://www-naweb.iaea.org/napc/ih/GNIP/IHS_GNIP.html⟩ (2006).
12. Vuille, M., Werner, M., Bradley, R. S. & Keimig, F. Stable isotopes in precipitation in the Asian monsoon region. *J. Geophys. Res.* **110,** D23108, doi:10.1029/2005JD006022 (2005).
13. Kawahata, H., Nishimura, A. & Gagan, M. Seasonal change in foraminiferal production in the western equatorial Pacific warm pool: evidence from sediment trap experiments. *Deep-Sea Res. II* **49,** 2783–2801 (2002).
14. Mohtadi, M. *et al.* Low-latitude control on seasonal and interannual changes in planktonic foraminiferal flux and shell geochemistry off south Java: a sediment trap study. *Paleoceanography* **24,** doi:10.1029/2008PA001636 (2009).
15. Thunell, R. C. & Reynolds, L. A. Sedimentation of planktonic foraminifera: seasonal changes in species in the Panama Basin. *Micropaleontology* **30,** 243–262 (1984).
16. Anand, P., Elderfield, H. & Conte, M. H. Calibration of Mg/Ca thermometry in planktonic foraminifera from a sediment trap time-series. *Paleoceanography* **18,** doi:10.1029/2002PA000846 (2003).
17. Lea, D. W., Pak, D. K. & Spero, H. J. Climate impact of late Quaternary equatorial Pacific sea surface temperature variations. *Science* **289,** 1719–1724 (2000).
18. Stott, L. *et al.* Decline of western Pacific surface ocean salinity and temperature in the early Holocene. *Nature* **431,** 56–59 (2004).
19. Rosenthal, Y., Oppo, D. W. & Linsley, B. K. The amplitude and phasing of climate change during the last deglaciation in the Sulu Sea, western equatorial Pacific. *Geophys. Res. Lett.* **30,** doi:10.1029/2002GL016612 (2003).
20. Moy, C. M., Seltzer, G. O., Rodbell, D. T. & Anderson, D. M. Variability of El Niño/Southern Oscillation activity at millennial timescales during the Holocene epoch. *Nature* **420,** 162–165 (2002).
21. Conroy, J. L., Overpeck, J. T., Cole, J. E., Shanahan, T. M. & Steinitz-Kannan, M. Holocene changes in eastern tropical Pacific climate inferred from a Galapagos lake sediment record. *Quat. Sci. Rev.* **27,** 1166–1180 (2008).
22. Gordon, A. L., Susanto, R. D. & Vranes, K. Cool Indonesian throughflow as a consequence of restricted surface layer flow. *Nature* **425,** 824–828 (2003).
23. Zhang, P. *et al.* A test of climate, sun, and culture relationships from an 1810-year Chinese cave record. *Science* **322,** 940–942 (2008).
24. Yancheva, G. *et al.* Influence of the intertropical convergence zone on the East Asian monsoon. *Nature* **445,** 74–77 (2007).
25. Sontakke, N. A., Pant, G. B. & Singh, N. Construction of all-India summer monsoon rainfall series for the period 1844–1991. *J. Clim.* **6,** 1807–1811 (1993).
26. Haug, G. H. *et al.* Southward migration of the Intertropical Convergence Zone through the Holocene. *Science* **293,** 1304–1308 (2001).
27. Wang, Y. *et al.* The Holocene Asian monsoon: links to solar changes and North Atlantic climate. *Science* **308,** 854–857 (2005).
28. Barsugli, J. J. & Sardeshmukh, P. D. Global atmospheric sensitivity to tropical SST anomalies throughout the Indo-Pacific basin. *J. Clim.* **15,** 3427–3442 (2003).
29. Locarnini, R. A., Mishonov, A. V., Antonov, J. I., Boyer, T. P. & Garcia, H. E. *World Ocean Atlas 2005* Vol. 1, *Temperature* (ed. Levitus, S.) (NOAA Atlas NESDIS 61, US Govt Printing Office, 2006).

Supplementary Information is linked to the online version of the paper at www.nature.com/nature.

Acknowledgements We thank the following people and institutions for their support: Y. S. Djajadihardja, F. Syamsudin, the captain and crew of our 2003 RV *Baruna Jaya VIII* cruise, the Indonesian Agency for Assessment and Application of Technology (BPPT), and the Center of Research and Development for Oceanography (LIPI) of Indonesia. This work was financially supported by the US NSF and the Ocean Climate Change Institute of WHOI. We thank L. Zou, D. Ostermann, K. Rose, S. Pike and M. Chong for technical assistance, W. Martin, O. Marchal, C. Saenger and K. Dahl for discussions, and the NOSAMS and Radioanalytical facilities at WHOI for radiocarbon and ^{210}Pb analyses, respectively.

Author Contributions All authors contributed extensively to this work.

Author Information Data are available at ftp://ftp.ncdc.noaa.gov/pub/data/paleo/contributions_by_author/oppo2009/oppo2009.txt. Reprints and permissions information is available at www.nature.com/reprints. Correspondence and requests for materials should be addressed to D.W.O. (doppo@whoi.edu).

SUPPLEMENTARY INFORMATION

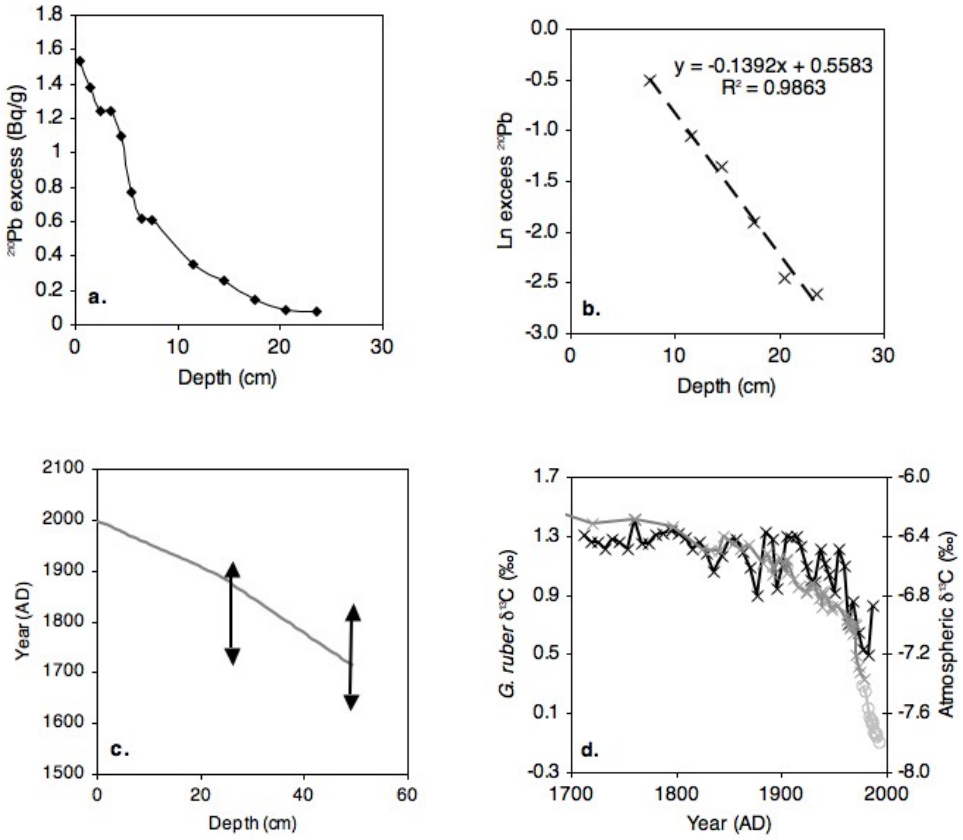

Supplementary Figure 1. Age control for MC31A. **a,** MC31A $^{210}Pb_{excess}$ versus depth**. b,** Regression of the natural log of $^{210}Pb_{excess}$ from depths below the sediment mixed layer, between 7.5 and 23.5 cm, versus depth. **c,** Assumed age versus depth relationship (line) yielded age estimates that were within error of ages suggested by radiocarbon data (vertical arrows indicate (±1σ error bars). **d,** Low $\delta^{13}C$ values of *G. ruber* at the top of the core (black) are consistent with the recent decrease in atmospheric $\delta^{13}C$ (grey)[37,38]. A bequerel: 1 Bq=1 decay/second.

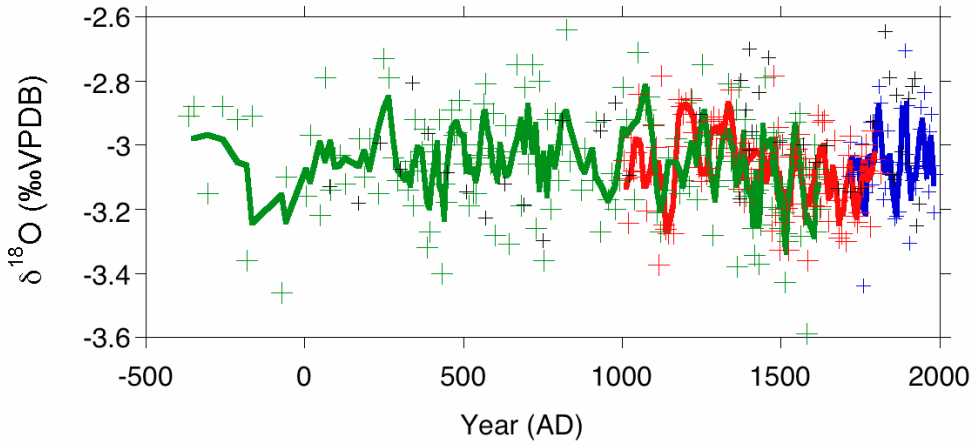

Supplementary Figure 2. *G. ruber* δ^{18}O data. Comparison of δ^{18}O records after corrections for offsets**.** Black, 32GGC; Blue, 31MC; Green, 34GGC; Red, MD60[7]. Data and 3-point running means. δ^{18}O values are relative to Vienna PeeDee Belemnite (VPDB).

Supplementary Table 1. Radiocarbon Dates. All measurements were made at the National Ocean Sciences Accelerator Mass Spectrometry Facility (NOSAMS) on mixed planktonic foraminifera and converted to calendar age[34] using a reservoir age of 475 years[35].

Core	ID	Depth (cm)	^{14}C Age±1σ	Calendar age ±1σ (BP)
MC31A	OS-45713	0-1	>Modern	*
MC31A	OS-58731	26-27	620±30	138±94
MC31A	OS-52863	49-50	675±45	232±95
32GGC	OS-52745	3.5-4.5	45±40	*
32GGC	OS-57846	70.5-71.5	920±30	503±14
32GGC	OS-54078	135.5-136.5	1140±30	639±34
32GGC	OS-57776	179.5-180.5	1610±35	1034±44
32GGC	OS-54079	229.5-230.5	2210±30	1644±46
32GGC	OS-57777	275.5-276.5	2460±35	1928±38
34GGC	OS-52741	8.5-9.5	780±55	358±79
34GGC	OS-52742	103.5-104.5	1320±40	748±43
34GGC	OS-52743	199.5-200.5	1900±45	1320±30
34GGC	OS-52733	303.5-304.5	2270±45	1719±59
34GGC	OS-45717	380-381	2750±30	2308±43

*Outside calibration range.

Supplementary Table 2. ^{210}Pb and ^{214}Pb measurements for MC31.

Depth, cm	^{210}Pb, Bq/g	^{214}Pb, Bq/g
0-1	1.5745	0.0395
1-2	1.4219	0.0416
2-3	1.2811	0.0380
3-4	1.2833	0.0407
4-5	1.1375	0.0404
5-6	0.8126	0.0387
6-7	0.6544	0.0395
7-8	0.6455	0.0394
11-12	0.3838	0.0325
14-15	0.2887	0.0317
17-18	0.1823	0.0325
20-21	0.1177	0.0318
23-24	0.1065	0.0331

Supplementary Discussion

Seasonal surface variability

Surface temperatures are lowest in boreal summer, when monsoon winds drive regional upwelling and advection of cold, upwelled waters from the south (Supp. Fig. 3). Regional surface waters are freshest in boreal winter[41], when the Intertropical Convergence Zone (ITCZ) is near or above the site (precipitation averages 9-11mm/day)[9] and surface currents advect low salinity waters from the east[42]. During boreal summer, the ITCZ rainfall migrates northward so rainfall over the site decreases (~2-3 mm/day), and southward flowing surface currents bring higher salinity Pacific waters to the site[42]. Thus, under modern conditions, surface waters are colder and saltier in boreal summer, and warmer and fresher during boreal winter.

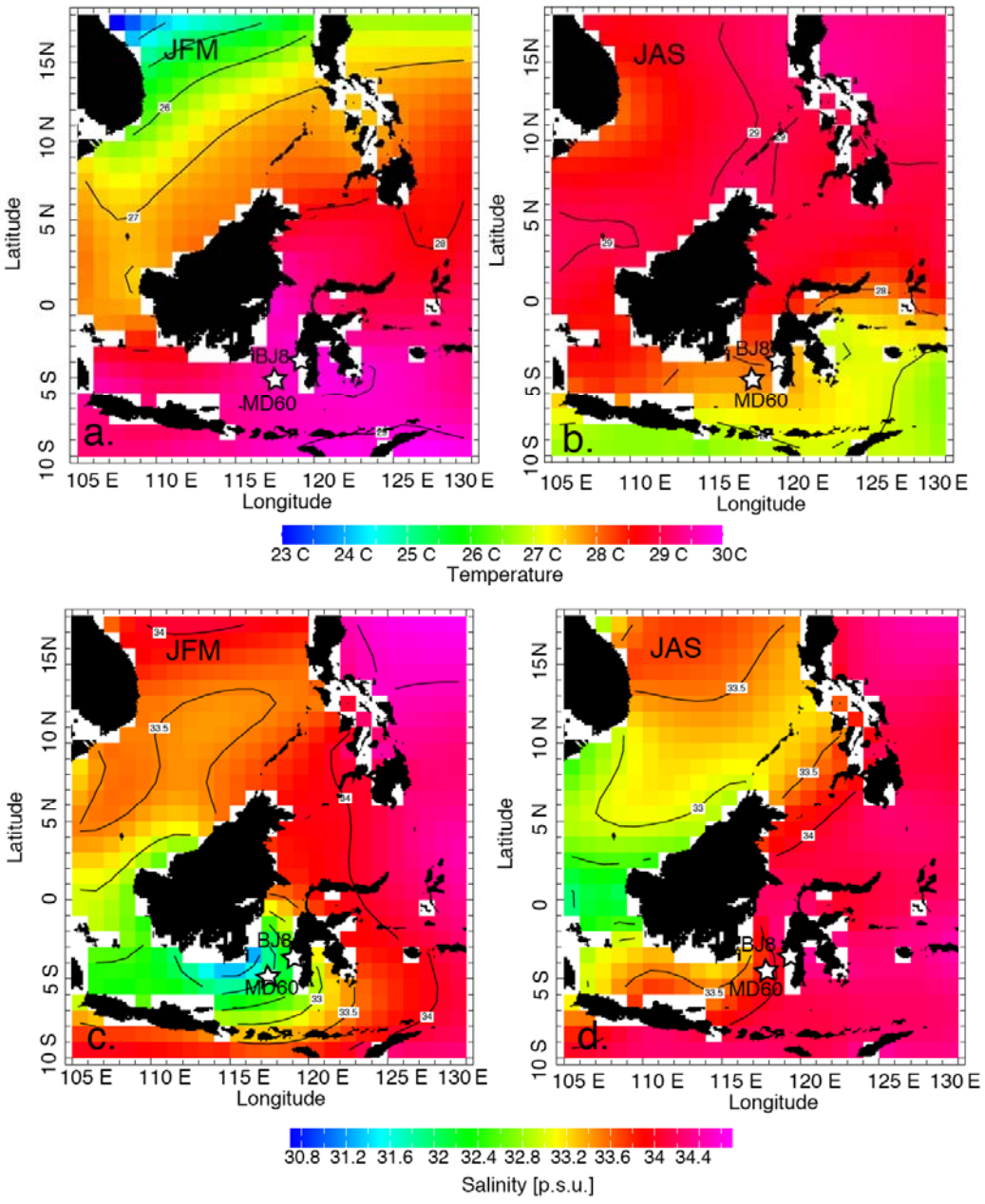

Supplementary Figure 3. **Seasonal surface variability.** Boreal winter (a, c) and summer (b, d) SST[8] and SSS[41] for study area. Core locations denoted by stars.

Seasonality of *G. ruber* flux to the sediment

Data from two of three sediment traps from the IPWP suggest that ~50% of the flux of *G. ruber* to the sediment occurs in association with upwelling of colder, nutrient-rich water during the boreal summer monsoon[15,16] with the remainder occurring during warmer times of the year. Data from a third IPWP trap suggest that *G. ruber* lives throughout the year in approximately constant abundance[14]. In the Panama Basin, eastern equatorial Pacific, the flux of *G. ruber* during the establishment of a deep warm mixed layer is 2-3 times larger than that during the upwelling season[16]. Sediment trap studies from the western Arabian Sea indicate that *G. ruber* seasonality is highly sensitive to upwelling intensity but that there are spatial variations in the response of *G. ruber* to upwelling. *G. ruber* fluxes increase within the margins of the upwelling region during the summer monsoon[43, 44]. Offshore, the *G. ruber* fluxes also increased during the upwelling season[43,44]. Close to shore in the center of the upwelling system, however, the flux of *G. ruber* did not increase during the upwelling season[43]. These data suggest that at least in some tropical locations, the flux of *G. ruber* to the sediment is highest during either non-upwelling or marginal upwelling conditions.

Relationship between Indonesian and Global temperature trends

In order to evaluate how well Indonesian SSTs have tracked global mean SSTs from AD 1856-1991 on multi-decadal and longer time scales, we correlated a 40-year averaged global mean annual SST index (30°S-60°N) to 40-year averaged SSTs throughout the world's oceans[45] (Supp. Fig. 4). The correlation analysis suggests that SST in our study area is strongly correlated to global SSTs ($r>0.8$) on this time scale.

How well Indonesian SST tracks multi-decadal land temperatures depends on which of two historical SST reconstructions[8,45] is more accurate (Supp. Fig. 5). However, the increase of mean annual SST since AD 1900 in both reconstructions is similar to the rise of NH and global land temperature since AD 1900[46].The greater down-core amplitude of reconstructed Indonesian SST variations than reconstructed NH surface air temperature variations (Fig. 3a), therefore, may be related to changes in *G. ruber* seasonality.

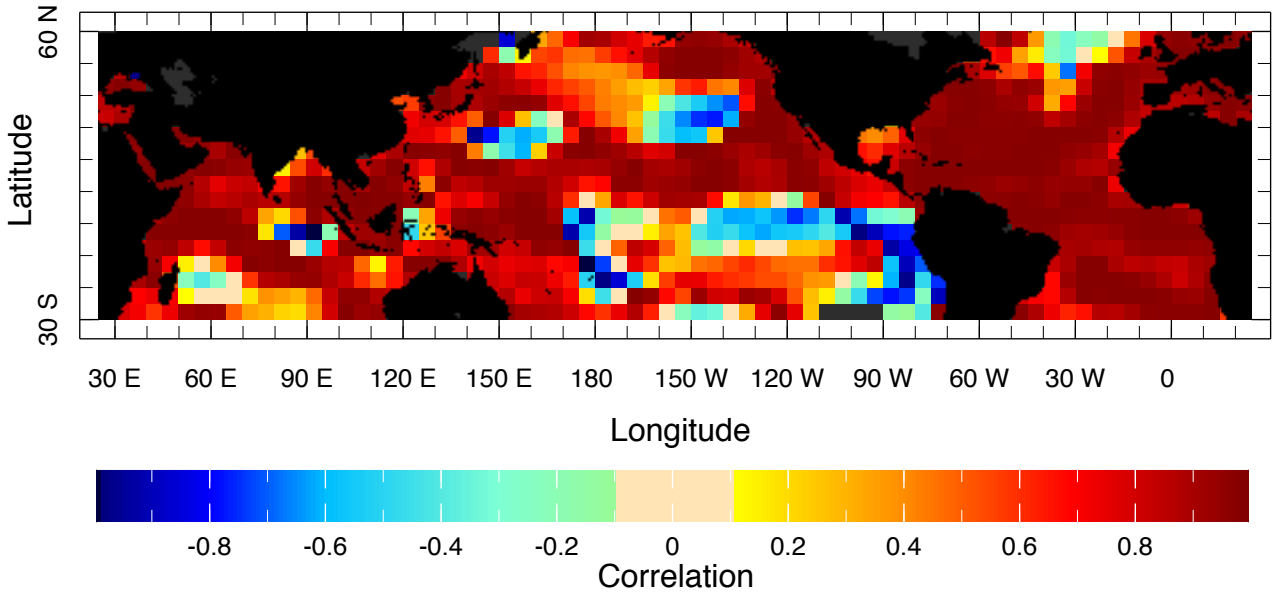

Supplementary Figure 4. Correlation between 40-year averaged global mean SST and local SST[45].

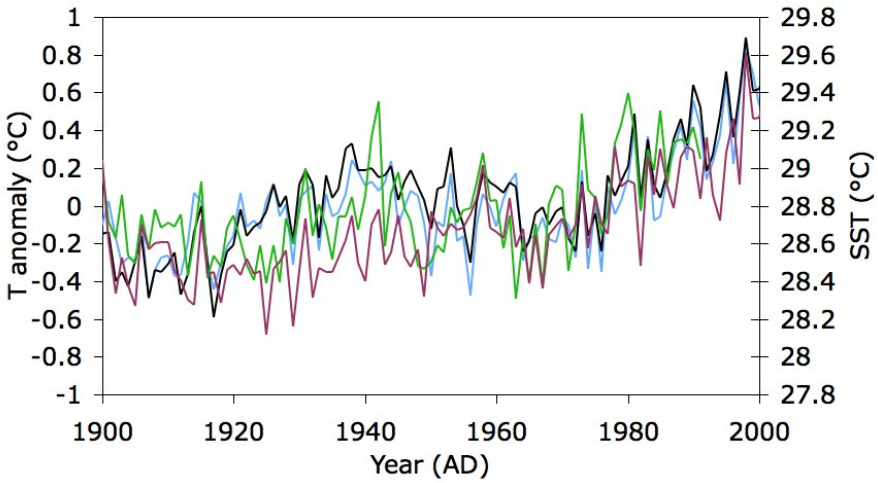

Supplementary Figure 5. Temperature reconstructions. Historical mean annual SST reconstructions (purple[8] and green[45]) compared to NH (black) and global (blue) land temperature anomaly reconstructions[46].

Relationship between Indonesian JAS and mean annual SST

Because our Mg/Ca-based SST estimates suggest that the seasonality of *G. ruber* changes on decadal and longer time scales (Fig. 2a), we compared JAS SSTs to SSTs during the rest of the year (October through June)[8]. Multi-taper spectral analysis using a Matlab script written by Dr. Peter Huybers (http://www.people.fas.harvard.edu/~phuybers/Mfiles/index.html) indicates that JAS SST variations are coherent and in phase with SST during the rest of the year on decadal and longer time scales (Supp. Fig. 6), suggesting that our reconstructed SST on decadal and longer time scales also reflects mean annual SST trends, although with higher amplitude. In order to estimate mean annual LIA SST relative to 1997-2007, we linearly regressed historical JAS SST against mean annual SST (1856-2007)[8] (Supp. Fig. 7). The results suggest, that on average, and across all represented time scales, mean annual SSTs at our study site have an amplitude ~70% of JAS SSTs (r^2=0.75, p<<0.0001). As our SST reconstruction suggests that peak LIA JAS SSTs were ~ 1°±0.2°C colder than the 1997-2007 mean (Fig. 2b, 3a), the slope of the regression suggests that peak LIA mean annual SST's were ~0.7°C colder (or less than 1°C colder) than the 1997-2007 mean.

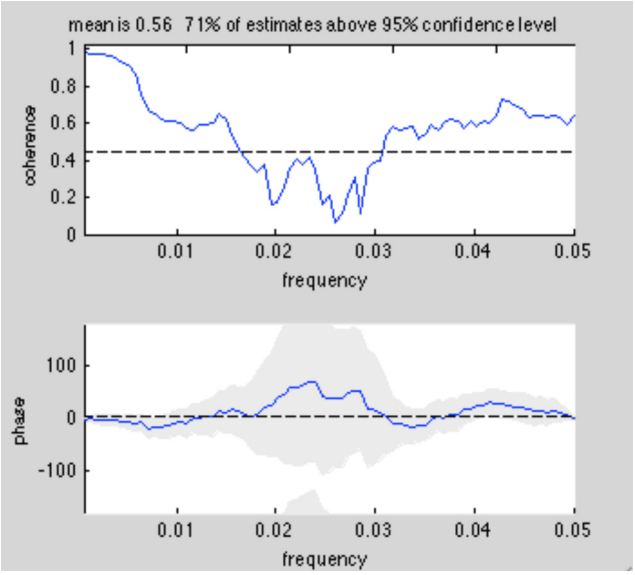

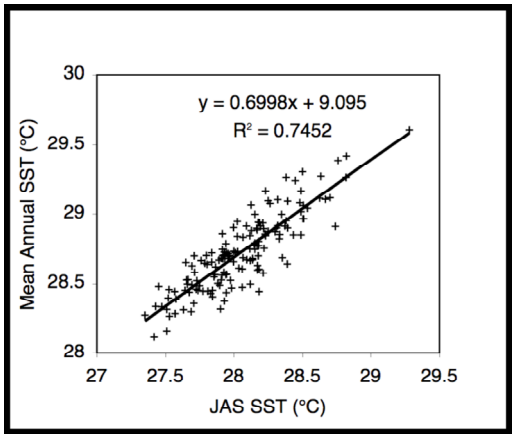

Supplementary Figure 6. Cross-spectral analysis between JAS and October-June SST[9]. Frequency is in cycles per year.

Supplementary Figure 7. Regression between JAS and mean annual SST[9].

References:

41. Antonov, J. I., Locarnini, R. A., Boyer, T. P., Mishonov, A. V. & Garcia H. E. World Ocean Atlas 2005, Volume 2: Salinity. S. Levitus, Ed. NOAA Atlas NESDIS 62, U.S. Government Printing Office, Washington, D.C., 182 pp. (2006).

Data available at http://iridl.ldeo.columbia.edu/SOURCES/.NOAA/.NODC/.WOA05/

42. Gordon, A. L., Susanto, R. D. & Vranes, K. Cool Indonesian throughflow as a consequence of restricted surface layer flow. *Nature* **425**, 824–828 (2003).

43. Schiebel, R. *et al*. Distribution of diatoms, coccolithophores and planktic foraminifers along a trophic gradient during SW monsoon in the Arabian Sea. *Marine Micropaleontology* ***51***, 345–371 (2004).

44. Curry, W. B., Ostermann, D. R., Guptha, M. V. S. & Ittekkot V. Foraminiferal production and monsoonal upwelling in the Arabian Sea: evidence from sediment traps, in *Upwelling Systems: Evolution Since the Early Miocene*, edited by Summerhayes, C. P. Prell, W. L. & Emeis, K. C. pp. 93–106, No. 64 in Geological Society Special Publication, London (1992).

45. Kaplan, A., Cane, M., Kushnir, Y., Clement, A., Blumenthal, M., & Rajagopalan, B. Analyses of global sea surface temperature 1856-1991. *J. of Geophys. Res*. **103**, 18,567–18,589 (1998).

46. Hansen, J., Ruedy, R., Glascoe, J., & Sato, M. GISS analysis of surface temperature change. *J. Geophys. Res*. **104**, 30997-31022 (1999). Data available at http://data.giss.nasa.gov/gistemp/.